

Monodispersed Hollow SO₃H-Functionalized Carbon/Silica as Efficient Solid Acid Catalyst for Esterification of Oleic Acid

Yang Wang,[†] Ding Wang,[‡] Minghui Tan,^{†,§} Bo Jiang,[†] Jingtang Zheng,[†] Noritatsu Tsubaki,^{*,§} and Mingbo Wu^{*,†}

[†]State Key Laboratory of Heavy Oil Processing, China University of Petroleum, Qingdao 266580, China

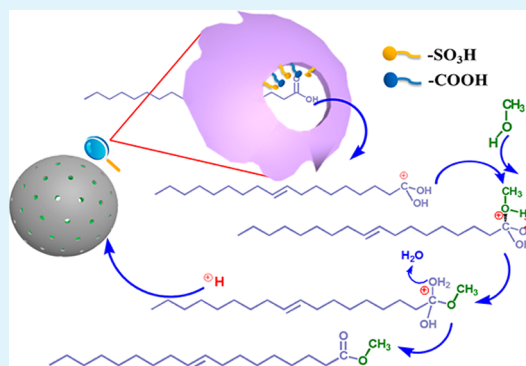
[‡]College of Materials Science and Engineering, University of Shanghai for Science & Technology, Shanghai 200093, China

[§]Department of Applied Chemistry, Graduate School of Engineering, University of Toyama, Gofuku 3190, Toyama 930-8555, Japan

Supporting Information

ABSTRACT: SO₃H-functionalized monodispersed hollow carbon/silica spheres (HS/C-SO₃H) with primary mesopores were prepared with polystyrene as a template and *p*-toluenesulfonic acid (TsOH) as a carbon precursor and –SO₃H source simultaneously. The physical and chemical properties of HS/C-SO₃H were characterized by N₂ adsorption, TEM, SEM, XPS, XRD, Raman spectrum, NH₃-TPD, element analysis and acid–base titration techniques. As a solid acid catalyst, HS/C-SO₃H shows excellent performance in the esterification of oleic acid with methanol, which is a crucial reaction in biodiesel production. The well-defined hollow architecture and enhanced active sites accessibility of HS/C-SO₃H guarantee the highest catalytic performance compared with the catalysts prepared by activation of TsOH deposited on the ordered mesoporous silicas SBA-15 and MCM-41. At the optimized conditions, high conversion (96.9%) was achieved and no distinct activity drop was observed after 5 recycles. This synthesis strategy will provide a highly effective solid acid catalyst for green chemical processes.

KEYWORDS: hollow, carbon/silica composite, solid acid catalyst, esterification, biodiesel



1. INTRODUCTION

With the diminishing of crude oil reserves and environmental deterioration, the exploration of alternative energy is an effective way to realize sustainable development. Special attention has been paid to biomass-derived energy due to its abundant, renewable and environmental friendly. Biodiesel regarded as a potential substitute to petroleum-derived diesel is composed of fatty acid methyl esters (FAMES) produced via the base-catalyzed transesterification of triglyceride.^{1,2} However, current biodiesel production has low energy efficiency due to lots of free fatty acids (FFAs) contained in feedstocks, which will neutralize the base catalysts and produce large amounts of soap.³ Therefore, acid-catalyzed pre-esterification of FFAs is essential to improve the energy efficiency. In addition, esterification and transesterification can be performed simultaneously under acid-catalyzed conditions.^{4–6}

Homogeneous acid catalysts, such as H₂SO₄, HCl and H₃PO₄, are widely used in industrial biodiesel production. However, some drawbacks such as corrosive to equipment, difficult to recycle and environmentally hazardous have limited their application. In recent years, solid acid catalysts have gained much attention due to their recyclable and environmental friendly properties. Solid acid catalysts such as sulfonated metal oxide,^{7–9} sulfonated resins,^{10,11} zeolite,^{12–14} and supported heteropoly acid catalysts^{15,16} have been

proposed to replace the homogeneous acid. However, some shortcomings such as low acid sites content, poor stability and high cost restrict their application in biodiesel production. The carbon-based solid acid catalyst has been proved to be a promising heterogeneous catalyst in the conversion of biomass due to its excellent hydrothermal stability and catalytic activity.^{17,18} In the past few years, researchers have developed a variety of solid acid catalysts based on carbon materials, such as incomplete carbonization of organic compounds,^{19,20} ordered mesoporous carbons,^{21–23} and carbon–silica composites.^{24–26} Unfortunately, the traditional solid acid catalysts are usually prepared by heating carbon materials under concentrated H₂SO₄, which will damage the structure of the carbon skeleton and is not a green synthesis method. *p*-Toluenesulfonic acid (TsOH) as a small molecule organic acid can be used as both a carbon precursor and –SO₃H source to produce a solid acid catalyst by a hydrothermal carbonization process²⁷ or chemical activation method,^{28,29} which is favorable to reduce the consumption of corrosive and hazardous concentrated H₂SO₄. One of the largest challenges to improve the catalytic performance of the solid acid catalyst is to improve the in-pore

Received: September 17, 2015

Accepted: November 13, 2015

Published: November 13, 2015

molecules diffusion and active sites accessibility. It is urgent to seek an ideal catalyst with superior mass diffusion property to enhance the catalytic activity of the catalyst significantly, especially for the reactions involving bulky FFA molecules.^{13,30}

Notably, hollow-structured mesoporous materials (HMM) have attracted great attention in various fields, such as catalysis,^{31–33} adsorption and separation,^{34,35} and energy storage owing to their outstanding features arising from the distinctive pore structure composed of a hollow core and a mesoporous shell.^{36,37} As a catalyst support, HMM can accelerate the mass-transport rate due to the mesopores in the shell, connecting the interior and exterior of the hollow core, and providing a highway for the free diffusions of reactants and products, respectively.³⁸ The active sites can be encapsulated into the cores^{39–41} or loaded on the shells⁴² of the HMM. Given the unique architecture and rapid mass transfer of HMM, solid acid catalysts with a mesoporous shell and hollow cavity should have superior performance in the field of catalysis.

In this study, a monodispersed hollow carbon/silica solid acid catalyst (HS/C-SO₃H) was prepared by chemical activation of the organic compound TsOH on the mesoporous shells of the hollow silica. As-made HS/C-SO₃H has a thin mesoporous shell with a connected interior and exterior surfaces, which can act as a nanoreactor to enhance the mass-transport process and catalytic performance. The -SO₃H functionalized carbon layers were also deposited on the ordered mesoporous silica SBA-15 and MCM-41 by the same method to verify the structure–function relationship of HS/C-SO₃H. The chemical and physical characteristics of obtained catalysts were systematically analyzed. The esterification of oleic acid with methanol was employed as a probe reaction to explore the enhanced catalytic performance derived from the unique architecture characteristics.

2. EXPERIMENTAL SECTION

2.1. Synthesis of Carbon/Silica Solid Acid Catalysts. Hollow silica (HS) and SBA-15 were synthesized via following procedures reported in the literature.^{43,44} Briefly, the polystyrene (PS) latex with diameter around 300 nm was first prepared by emulsion polymerization. Specially, 1.22 g of polyvinylpyrrolidone (K-30, AR, Aladdin Reagent Co., Ltd.) was dissolved in 790 g of distilled water under vigorous stirring. 80 g of styrene (AR, Sinopharm Chemical Reagent Co., Ltd.) was added, and the mixture was kept stirring under nitrogen purge for 30 min to form an emulsion. The emulsion was heated to 70 °C and 10 mL of aqueous solution containing 1.2 g of 2,2'-azobis(2-methylpropionamide)dihydrochloride (V-50, >97.0%, Aladdin Reagent Co., Ltd.) was then injected to initiate the polymerization. The emulsion was then polymerized for 24 h under nitrogen to form the latex. HS was then prepared using above synthesized PS latex as a hard template. Typically, 25 g of PS latex was added dropwise to a mixture of 0.8 g of hexadecyltrimethylammonium bromide (CTAB, AR, Sinopharm Chemical Reagent Co., Ltd.), 9.6 g of water, 11.0 g of ethanol and 2.0 mL of ammonium hydroxide solution under vigorous stirring. The mixture was sonicated for 10 min and magnetically stirred for 30 min before adding dropwise 1.5 g of tetraethoxysilane (TEOS, AR, Aladdin Reagent Co., Ltd.). The mixture was kept at room temperature for 48 h before the mesoporous silica coated latex was recovered by centrifugation, followed by washing with ethanol. The precipitate was dried in the air overnight and calcined at 600 °C to remove the template. To synthesize the SBA-15, 2 g of Pluronic P123 (Aldrich) was dissolved in 75 mL of 1.6 M aqueous HCl solution at 40 °C before 4.3 g of TEOS was added. The mixture was stirred at 40 °C for 20 h and transferred to an autoclave and heated at 100 °C for 48 h. The solid was collected by filtration, washed with distilled water and dried at 65 °C. The white solid was calcined at 550 °C for 8 h to

remove P123. MCM-41 was purchased from the Catalyst Plant of NanKai University.

The carbon/silica solid acid catalysts were prepared according to the procedure reported in the literature.^{28,29} Specially, 1.3 g of *p*-toluenesulfonic acid (TsOH, AR, Sinopharm Chemical Reagent Co., Ltd.) was dissolved in acetone before 0.5 g of silica was added. The suspension was sonicated for 1 h, stirred for 24 h at room temperature and heated at 100 °C for 6 h and then at 160 °C for 6 h. The solid was suspended in 5 mL of 2.5 M H₂SO₄ solution, and the mixture was stirred for 24 h at room temperature. The water contained in the suspension was evaporated at 110 °C, and the acid impregnated solid was heated at 250 °C in a tubular furnace under a N₂ flow for 1 h. The carbon/silica composites was washed with distilled water (until neutral pH) followed by acetone, and dried at 65 °C. The samples produced with HS, SBA-15 and MCM-41 as supports are denoted as HS/C-SO₃H, SBA-15/C-SO₃H and MCM-41/C-SO₃H, respectively.

2.2. Characterization. The powder X-ray diffraction (XRD) patterns of the catalysts were characterized with a PANalytica X'Pert PRO X-ray diffractometer using Cu K α radiation. Fourier transform infrared (FT-IR) were measured with a NEXUS FT-IR spectrometer in the range of 400–4000 cm⁻¹. The surface area and pore size distribution of the solid acid catalyst were measured with a Micromeritics ASAP 2020 M instrument. All samples were degassed at 200 °C prior to measurements. The specific surface area was calculated by the Brunauer–Emmett–Teller (BET) method, and the pore size and pore volume were calculated according to the Barrett–Joyner–Halenda (BJH) formula. The pore size distribution was calculated by the density functional theory (DFT) method based on nitrogen adsorption. The microstructures and morphologies of the samples were recorded with a JEM-2100UHR transmission electron microscopy (TEM) instrument and a Hitachi S-4800 field emission scanning electron microscopy (FE-SEM) instrument. Raman measurements were carried out on a Jobin-Yvon Labram-010 Raman spectrometer. X-ray photoelectron spectroscopy (XPS) analysis was performed on a ULVAC-PHI 5000 VersaProbe X-ray photoelectron spectroscopy system. Thermogravimetric analysis (TGA) was performed under air flow from room temperature to 800 °C, with a heating rate of 10 °C/min, on a STA 409 PC Luxx. C, H and S analyses of the catalysts were carried out by combustion in a Elementar Vario EL III elemental analyzer equipped with a TCD detector. NH₃ temperature-programmed desorption (NH₃-TPD) measurements were conducted on a Micromeritics AutoChem HP 2950 equipped with a thermal conductivity detector. Prior to the analysis, samples were pretreated at 150 °C for 1 h in a flow of ultrapure helium gas, and then cooled to 50 °C. The pretreated samples were saturated with 10% anhydrous ammonia gas for 30 min. Then the physically adsorbed NH₃ was removed by helium gas. The TPD experiments were performed in the temperature range of 50 to 400 °C at a heating rate of 10 °C min⁻¹. To compare the intensity difference of the acid sites, the catalysts with same weight were employed to perform the NH₃-TPD experiments.

The total acid densities of the catalysts were determined by acid–base titration.²⁹ 150 mg of catalyst was added to NaCl solution (20 mL, 0.1 M). After the solution was stirred for 24 h, the solid was separated from the solution by filtration. Then the filtrate was titrated to an end point at pH of 7 with 0.01 M NaOH. The total acid densities of the catalysts were estimated by calculating the amount of NaOH consumed.

2.3. Catalytic Tests. The catalytic performances of obtained solid acid catalysts were carried out at 80 °C in the esterification of oleic acid with methanol in a flask equipped with a reflux condenser, an oil bath and a magnetic stirrer. Typically, 0.1 g of solid acid catalyst was added to 2.8 g of oleic acid and 4 mL of methanol. After given reaction times, the catalysts were separated from the solution by centrifugation, and the product was separated with a rotary evaporator and diluted with *n*-hexane. The yield of methyl oleate was analyzed by gas chromatography (PerkinElmer Clarus 580 series) equipped with a flame ionization detection (FID) detector and a HP-5 capillary column, and methyl heptadecanoate (GC standard, Aldrich) was used as the internal standard. The conversion of oleic acid was calculated as

Conv. (%) = $m_{(\text{MO})} \times 100\% / m$, where Conv. (%) is the conversion of oleic acid, $m_{(\text{MO})}$ is the amount of methyl oleate and m is the amount of initial oleic acid.

The reusability of HS/C-SO₃H was measured by repeating 5 cycles of the esterification of oleic acid under the same reaction conditions. The used catalyst was separated from the reaction system by centrifugation and washed repeatedly with ethanol and distilled water after each experiment. The washed catalyst was vacuum-dried at 65 °C.

3. RESULTS AND DISCUSSION

3.1. Preparation and Characterization of Carbon/Silica Solid Acid Catalysts. The hollow silica (HS) with mesoporous shell was prepared from tetraethoxysilane (TEOS) in weakly basic ethanol/water solution using polystyrene (PS) latex (see the SEM image in Figure 1a) as a hard template. As

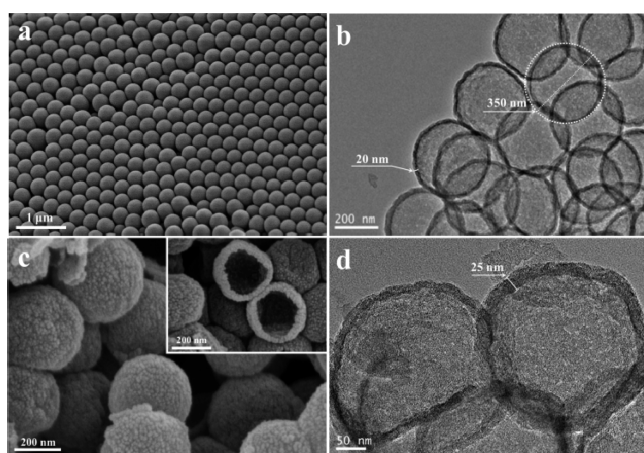


Figure 1. SEM images of PS latex (a) and HS/C-SO₃H (c); TEM images of HS (b) and HS/C-SO₃H (d).

shown in Figure 1b, the TEM image of HS presents well-defined hollow nanospheres with the diameter of about 350 nm and the shell thickness of around 20 nm.

As above-mentioned, HS/C-SO₃H was prepared by low temperature activation of TsOH (Scheme 1). TsOH provides both a carbon source and -SO₃H active sites in the shell of HS through incomplete carbonization. The mechanism for the

formation of HS/C-SO₃H is illustrated in Figure S1. TsOH was assembled on the surface of HS through hydrogen-bonding between the -SO₃H group of TsOH and the Si-OH group of HS.^{45,46} Then TsOH can be converted to the SO₃H-functionalized carbon layer by an acid-catalyzed dehydration reaction.⁴⁷ It is worth noting that the mesoporous shell of HS can accelerate the diffusion of TsOH to the interior surface of HS that guarantee the coating of SO₃H-functionalized carbon layer on the interior surface of HS. This phenomenon can be confirmed by the TEM image of HS/C-SO₃H in Figure S2. The formation of the SO₃H-functionalized carbon layer on the external and interior surfaces of HS will enhance the active site accessibility of the catalyst. With the same method, the functionalized carbon sheets were deposited onto the inner walls of SBA-15 and MCM-41 to compare and investigate the structure-function relationship of HS with mesoporous shell and hollow cavity. The weight percentage of the functionalized carbon component in the catalysts can be assessed by TGA (Figure S3 in the Supporting Information and Table 1). Furthermore, the element compositions of the functionalized carbon component in the catalysts were measured by element analysis (Table S1). After carbon depositing, the hollow catalyst HS/C-SO₃H spheres monodispersed as illustrated in Figure 1c. The TEM image of HS/C-SO₃H (Figure 1d) clearly discloses that the hollow spheres possess uniform shell thickness around 25 nm. The particle size of HS/C-SO₃H is about 355 nm (Figure S4), hence the increased particle size and shell thickness of HS demonstrate the successful attachment of the SO₃H-functionalized carbon layer to the shell of HS.

As-obtained HS exhibits a type IV N₂ adsorption and desorption isotherms (Figure 2a) with a notable H₄ type hysteresis loop due to the presence of mesoporous shell. The BET surface area, average pore size and pore volume of the mesoporous shell (Table 1) are 1254 m² g⁻¹, 5.0 nm and 0.96 cm³ g⁻¹, respectively. The TEM images (see Figure S5) and SAXRD patterns (Figure S6) of SBA-15 and MCM-41 suggest that silica possess periodic arrangements of mesopores with 2-d hexagonal structure. Compared to HS, the N₂ adsorption and desorption isotherms of HS/C-SO₃H in Figure 2a also belong to type IV with an obvious H₄ type hysteresis loop; however, the N₂ adsorption amount is less, which due to some space in the mesoporous shell has been occupied by coated carbon.

Scheme 1. Schematic Illustration of the Synthesis Process of HS and the Corresponding Carbon/Silica Solid Acid Catalyst HS/C-SO₃H

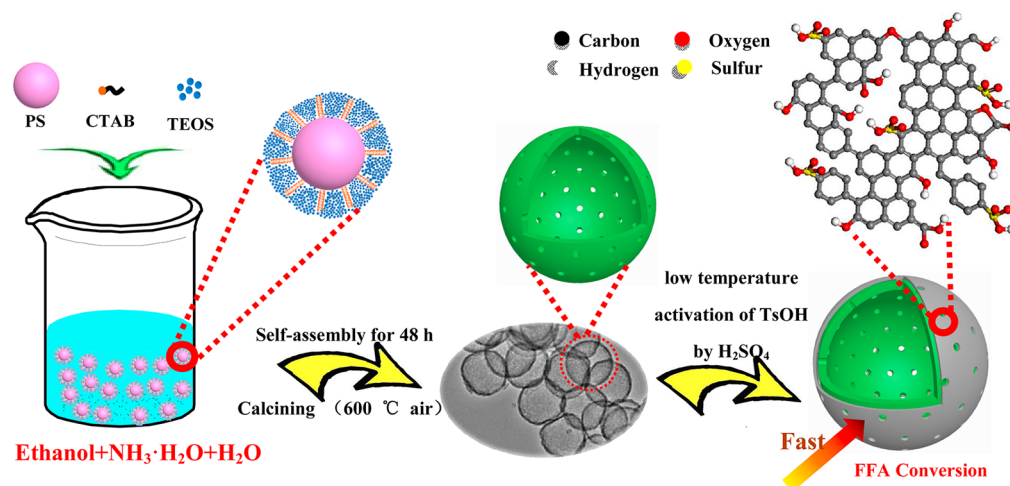
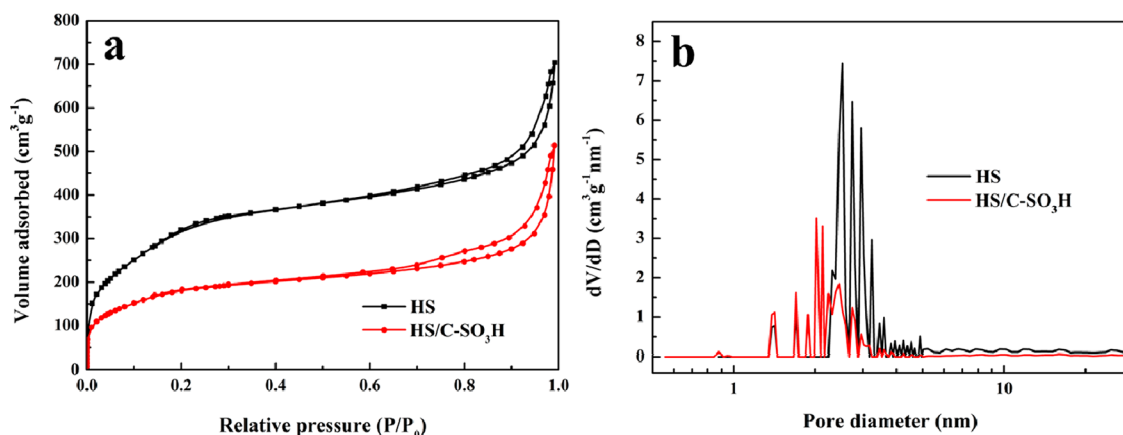


Table 1. Chemical and Textural Properties of the Silica and Catalysts, and the Catalytic Performances of the Catalysts

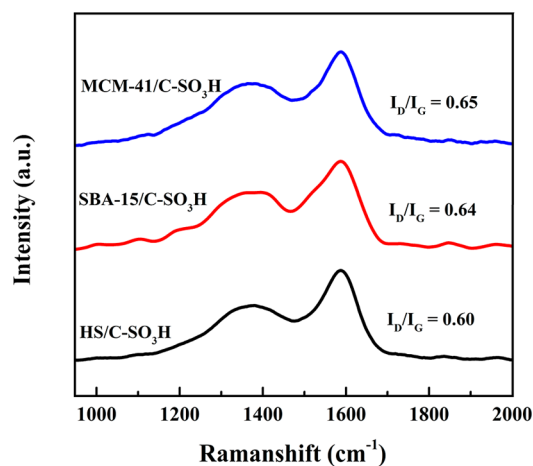
sample	coating (wt %) ^a	S_{BET} ($\text{m}^2 \text{g}^{-1}$) ^b	D (nm) ^c	V ($\text{cm}^3 \text{g}^{-1}$) ^d	total acid density ($\text{mmol H}^+ \text{g}^{-1}$) ^e	Conv. (%) ^f
HS		1254	5.0	0.96		
HS/C-SO ₃ H	40	470	4.2	0.40	2.10	96.9
SBA-15		849	5.0	1.00		
SBA-15/C-SO ₃ H	45	418	4.3	0.48	2.23	85.2
MCM-41		1060	2.9	0.92		
MCM-41/C-SO ₃ H	52	517	2.7	0.34	2.18	78.3
H ₂ SO ₄					20.4	98.0

^aWeight % of the functionalized carbon component assessed by TGA. ^bSpecific surface area estimated by the BET method. ^cAverage pore diameter estimated by BJH formula. ^dPore volume estimated by BJH formula. ^eAmount of acid sites measured by acid–base titration. ^fConversion of oleic acid. Reaction conditions: 2.8 g oleic acid, 4 mL methanol, 0.1 g catalyst, and 80 °C for 5 h.

**Figure 2.** N₂ adsorption and desorption isotherms (a); pore size distribution of HS and HS/C-SO₃H (b).

Correspondingly, the BET surface area, pore size and pore volume of HS/C-SO₃H are also less than those of HS. Nevertheless, the pore size of HS/C-SO₃H still keeps in the mesopore range, which can provide a free diffusion path for reactants and products. The texture properties of solid acid catalysts supported on SBA-15 and MCM-41 were also studied (Figure S5 and Table 1). The thickness of carbon layers deposited in the pores of SBA-15 and MCM-41 can be estimated from the difference between the pore sizes of catalysts and the original silica. The thicknesses of the carbon layers of SBA-15/C-SO₃H and MCM-41/C-SO₃H are 0.34 and 0.2 nm, respectively. Furthermore, the narrower pore size of MCM-41 compared to SBA-15 results in more functionalized carbon sheets deposited on the external surface of silica instead of inside pores. This phenomenon is also observed in SAXRD patterns in Figure S6. Compared to the diffraction peak intensity of SBA-15/C-SO₃H, MCM-41/C-SO₃H decreases dramatically due to the partial pores of silica being blocked by coated carbon sheets, which may hinder the transport of reactants and products.

As shown in Figure 3, the Raman spectra of all carbon/silica solid acid catalysts have two remarkable bands at 1360 cm⁻¹ (D-band) and 1586 cm⁻¹ (G-band). Because of the increase of ordered structure induced by more H₂SO₄ entering into the pores to promote the activation process at low temperature, HS/C-SO₃H exhibits the lowest peak intensity ratio of the D and G bands ($I_{\text{D}}/I_{\text{G}} = 0.60$) as compared to 0.64 of SBA-15/C-SO₃H and 0.65 of MCM-41/C-SO₃H. This phenomenon is also in accordance with the decreasing weight percent of carbon in TGA results as following sequence: MCM-41/C-SO₃H (52%) > SBA-15/C-SO₃H (45%) > HS/C-SO₃H (40%), in spite of the similar amount of TsOH usage. XRD patterns of

**Figure 3.** Raman spectra of the carbon/silica solid acid catalysts.

catalysts are shown in Figure S7. A characteristic diffraction peak (002) of amorphous carbon appeared at ca. 23°, which is overlapped with the diffraction peak of amorphous silica.

The FT-IR spectra of original silica and corresponding catalysts are shown in Figure 4. The different types of original silica contain typical vibration bands of Si—O—Si at 461, 806 and 1082 cm⁻¹. The typical band at 962 cm⁻¹ is assigned to the bending vibration of Si—OH groups. The —SO₃H functionalized carbon layers can be successfully deposited on original silica, which can be clearly seen from the emerged typical bands associated with carbon and its functional groups in FT-IR spectra. Typically, the bands around 1165, 1610 and 1710 cm⁻¹ are ascribed to C—O, C=C and C=O groups, respectively.

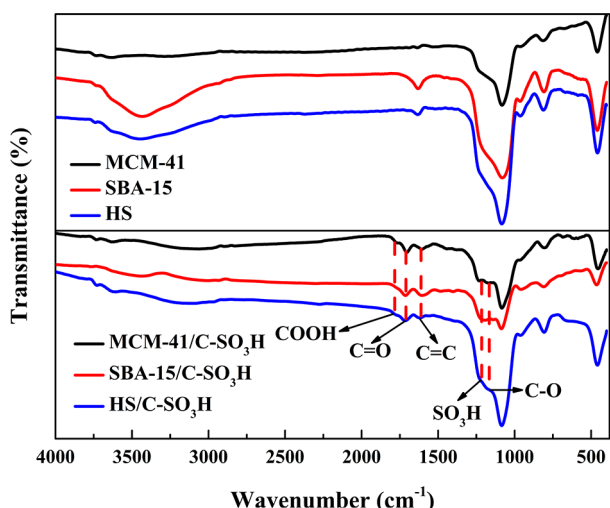


Figure 4. FT-IR spectra of the parent silica and corresponding carbon/silica solid acid catalysts.

The weak vibration bands at 1776 cm^{-1} is assigned to the stretching of $-\text{COOH}$ groups. These oxygen-containing functional groups are produced by the chemical activation of TsOH aided by the small amounts of H_2SO_4 . Furthermore, the band at 1220 cm^{-1} is attributed to the stretching mode of $-\text{SO}_3\text{H}$. The active sites ($-\text{SO}_3\text{H}$) of the catalysts originate from two contributions: the reservation of $-\text{SO}_3\text{H}$ existing in TsOH after the low temperature activation and the attachment of $-\text{SO}_3\text{H}$ provided by H_2SO_4 onto the carbon matrix during the chemical activation.

The XPS spectra in Figure 5a were used to clarify the surface chemical property of the catalysts. The XPS peaks of C 1s can be deconvoluted into two dominated components, i.e., C—C at 284.9 eV and C=C at 284.4 eV , along with two weaker bands associated with C=O (such as in carboxyl groups) at 288.7 eV and C—O (such as in hydroxyl groups) at 286.0 eV . The S 2p spectra in Figure 5b have two peaks at 167.6 and 163.3 eV assigned to sulfur in $-\text{SO}_3\text{H}$ and $-\text{SH}$ groups, respectively. Most sulfur exist in the form of $-\text{SO}_3\text{H}$, which is attributed to the strong oxidizing conditions in the chemical activation.²⁸ The emergence of $-\text{SH}$ groups are ascribed to the reduction of surface sulfonic acid groups to thiol groups at $250\text{ }^\circ\text{C}$. The relative amount of $-\text{SO}_3\text{H}$ on the surface of the catalysts can be

calculated roughly by the XPS data (Table S2) and results are as follows: MCM-41/C- SO_3H (4.0% , 1.25 mmol g^{-1}) > SBA-15/C- SO_3H (3.9% , 1.22 mmol g^{-1}) > HS/C- SO_3H (3.6% , 1.12 mmol g^{-1}). The FT-IR and XPS analysis results demonstrate the existence of a variety of acidic groups on the surface of the catalysts such as $-\text{SO}_3\text{H}$, $-\text{COOH}$ and $-\text{OH}$. Acid–base titration was employed to analyze further the acidic groups quantitatively (Table 1). It is noted that the amount of the strong acid sites ($-\text{SO}_3\text{H}$) of the carbon/silica solid acid catalysts synthesized by chemical activation procedure is comparable or even higher than those of conventional carbon-based solid acid catalysts, which are produced by the carbonization of a carbon precursor followed by a sulfonation process with concentrated H_2SO_4 (Table 2).

Table 2. Comparison of the Esterification of Oleic Acid with Methanol Catalyzed by HS/C- SO_3H and Other Catalysts Reported in Literature

catalyst	$S_{\text{BET}}^{\text{a}}$ ($\text{m}^2\text{ g}^{-1}$)	D (nm)	$-\text{SO}_3\text{H}$ density (mmol g^{-1})	Conv. (%)
HS/C- SO_3H (this work)	470	4.20	1.12	96.9
SC-Al-900 ^a	1118	8.16	1.86	77.7 ⁴⁹
Ca-648, 0.5-Sul-423,15 ^b			1.06	90.5 ⁵⁰
OMC- $\text{H}_2\text{O}_2\text{-SO}_3\text{H}^{\text{c}}$	475	3.50	1.86	86.0 ⁵¹
OMC-150- $\text{SO}_3\text{H}^{\text{d}}$	741	4.20	1.70	73.6 ²¹

^aReaction conditions: 1 g oleic acid, 8 mL methanol, 20 mg catalyst, and $65\text{ }^\circ\text{C}$ for 1.25 h. ^bReaction conditions: 2.8 g oleic acid, 4 mL methanol, $80\text{ }^\circ\text{C}$, 0.14 g catalyst and 5 h. ^cReaction conditions: 14 g oleic acid, 40 mL methanol, $80\text{ }^\circ\text{C}$, 0.1 g catalyst and 5 h. ^dReaction conditions: 1.4 g oleic acid, 2 mL methanol, $80\text{ }^\circ\text{C}$, 0.05 g catalyst and 10 h.

NH_3 -TPD analyses were carried out to clarify the acidic properties of the catalysts (Figure S8). The NH_3 -TPD profiles exhibit two peaks in the range of $50\text{--}400\text{ }^\circ\text{C}$. The peaks around 90 and $320\text{ }^\circ\text{C}$ can be attributed to the desorption of NH_3 from the weak ($-\text{OH}$, $-\text{COOH}$) and moderately strong ($-\text{SO}_3\text{H}$) Brønsted acid sites, respectively. What's more, a conclusion can be drawn from the intensity differences of the peaks that the intensity of $-\text{SO}_3\text{H}$ decreases as follows: MCM-41/C- SO_3H > SBA-15/C- SO_3H > HS/C- SO_3H , which is in accordance with the XPS results.

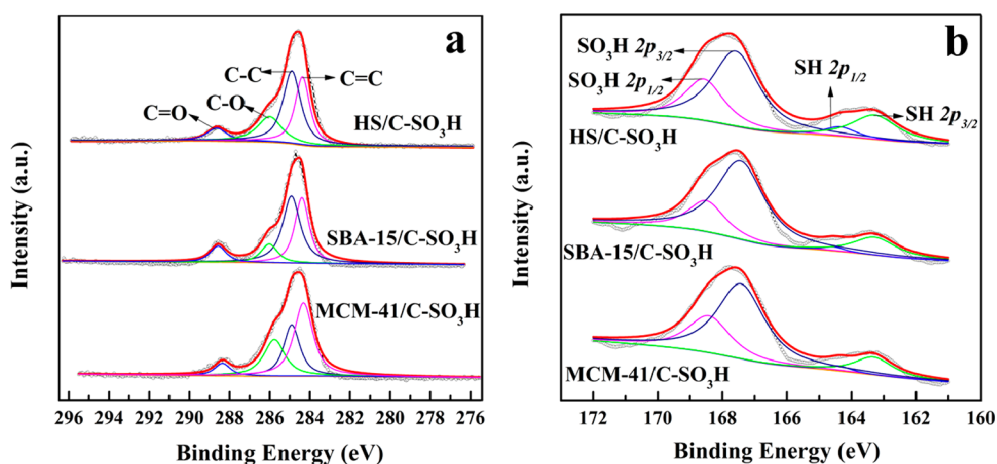
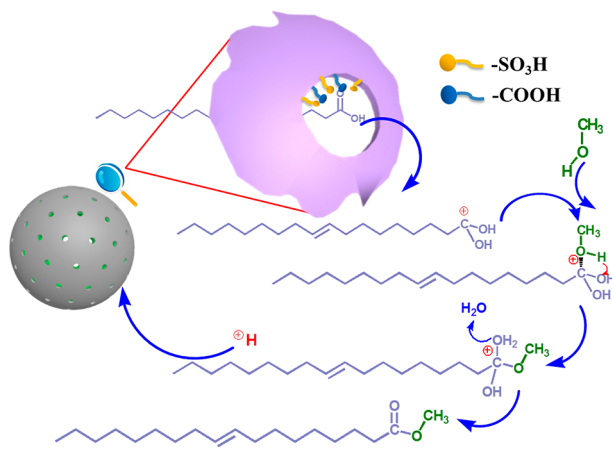


Figure 5. XPS spectra of C 1s (a) and S 2p (b) of the carbon/silica solid acid catalysts.

3.2. Catalytic Performance of Catalysts. The catalytic activities of the solid acid catalysts were evaluated through the esterification of oleic acid with methanol, which is one of the key reactions in biodiesel production. The mechanism for esterification of oleic acid with methanol by HS/C-SO₃H is shown in Scheme 2. Traditionally, the carbocation generated

Scheme 2. Catalytic Mechanism of the Esterification of Oleic Acid with Methanol by HS/C-SO₃H



from the interaction of carbonyl oxygen of oleic acid with the acidic site of the catalyst can be attacked by methanol. And this nucleophilic attack can produce a tetrahedral intermediate, which will eliminate H₂O to form methyl oleate. The active site can return back to the original form.⁴⁸ Figure 6 shows the

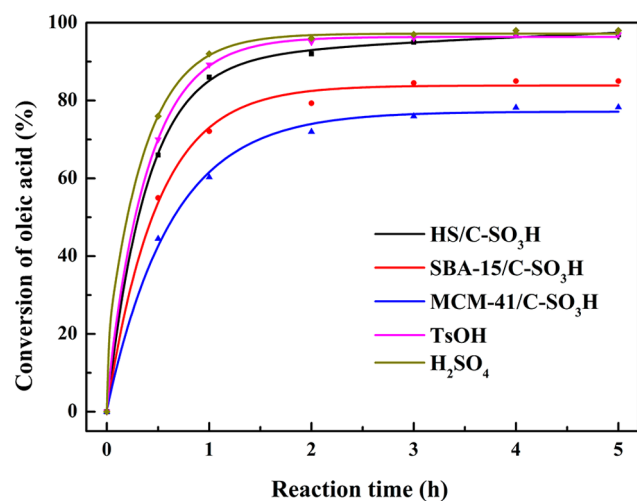


Figure 6. Catalytic performance of different catalysts. Reaction conditions: 2.8 g oleic acid, 4 mL methanol, 0.1 g solid acid catalyst or 5.5 mmol H₂SO₄, and 80 °C.

catalytic activities of the carbon/silica solid acid catalysts. The maximal conversions of all catalysts are obtained after 5 h with methyl oleate as the only product. MCM-41/C-SO₃H gives a yield of 78.3%, and the low activity is ascribed to the narrow pore size (2.7 nm), which hinders the mass transports of reactants and products. The higher yield of methyl oleate on SBA-15/C-SO₃H than on MCM-41/C-SO₃H (85.2% versus 78.3%) suggests that the good active sites accessibility is due to the larger pore size (4.3 nm versus 2.7 nm). HS/C-SO₃H shows much higher catalytic activity (96.9%) than other

supported ordered mesoporous silica catalysts in spite of its low content of active sites (1.12 mmol g⁻¹, calculated by XPS results) and small pore size and specific surface area (4.2 nm, 470 m² g⁻¹), which is even comparable to the traditional homogeneous catalysts H₂SO₄ and TsOH (98.0% and 97.1% after 5 h, respectively). Moreover, HS/C-SO₃H exhibits much higher catalytic activity in esterification of oleic acid than the other carbon-based solid acid catalysts in spite of the relative low -SO₃H density (Table 2). These enhanced catalytic performances are attributed to the unique hollow architecture with mesoporous shell, which can act as nanoreactor to accelerate the diffusions of reactants and products.

To verify further the structure–function relationship of the catalysts, the esterification reactions were performed at different MeOH/OA molar ratios (Figure 7). Because the esterification

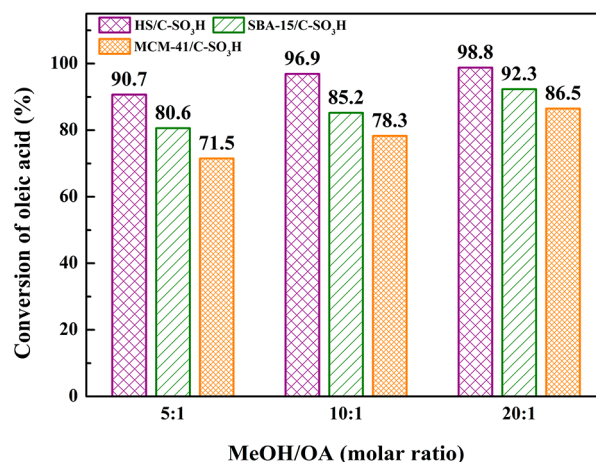


Figure 7. Effect of MeOH/OA molar ratio on the conversion of oleic acid. Reaction conditions: 2.8 g oleic acid, 4 mL methanol, 0.1 g solid acid catalyst, and 80 °C for 5 h.

is a reversible reaction, the increase of methanol will improve the conversion rate of the oleic acid, what is more, the increase of methanol will enhance the diffusion rate of the oleic acid, which is a long chain FFAs. HS/C-SO₃H exhibits more excellent catalytic performance (>90%) compared to SBA-15/C-SO₃H and MCM-41/C-SO₃H (80.6% and 71.5%, respectively) at low MeOH/OA molar ratio (5:1). As a long chain FFAs, oleic acid is difficult to diffuse in the long channels of SBA-15/C-SO₃H and MCM-41/C-SO₃H despite of their mesoporous structure, and the restriction effect will be magnified with the decreasing MeOH/OA molar ratio. For HS/C-SO₃H, the unique hollow structure and sphere shape can provide a free highway between the interior and exterior of the hollow core to enhance the molecular diffusion rate and active site accessibility. Therefore, the high catalytic activity of HS/C-SO₃H can be obtained even at low MeOH/OA molar ratio. When the MeOH/OA molar ratio is 20:1, the catalytic activities of SBA-15/C-SO₃H and MCM-41/C-SO₃H increase obviously, which are attributed to the good active site accessibility at higher MeOH/OA molar ratios. In conclusion, the fast mass-transport process of HS/C-SO₃H plays a vital role in the esterification process.

3.3. Reusability of the Catalysts. Figure 8 shows the reusability of HS/C-SO₃H through five cycles with MeOH/OA molar ratio of 10:1 at 80 °C and 5 h. The catalytic activity remains at a relatively stable value (>90%) after the conversion rate reduce gradually in the first three cycles, suggesting that

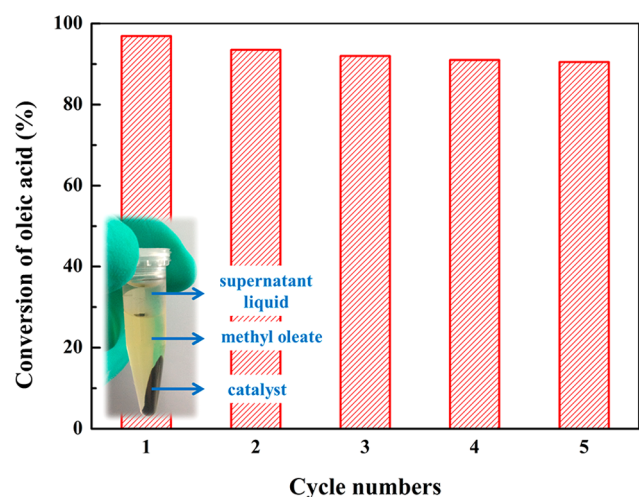


Figure 8. Recyclability of HS/C-SO₃H for the esterification of oleic acid. Reaction conditions: 2.8 g oleic acid, 4 mL methanol, 0.1 g solid catalyst, and 80 °C for 5 h. Inset: photograph of the centrifuged product.

HS/C-SO₃H are stable and can be recycled. To clarify the stability of HS/C-SO₃H, the element contents of HS/C-SO₃H after five cycles were determined by element analysis (Table S1). No obvious decrease of sulfur content (4.48%) of HS/C-SO₃H after five cycles further demonstrate its excellent reusability. We have also examined the HS/C-SO₃H under TEM observation after five cycles (Figure S9). The particle size and hollow structure of HS/C-SO₃H can be well retained after five cycles, which further corroborate the stability of HS/C-SO₃H. Furthermore, to test whether -SO₃H leached out into methyl oleate, the centrifuged methyl oleate was washed with water to extract -SO₃H possibly leached from the catalyst (see inset in Figure 8). A BaCl₂ precipitation test demonstrated that no -SO₃H existed in the washed water. The few leached out -SO₃H could exist in the supernatant liquid due to the hydrophilicity of -SO₃H. This chemical activation method can fabricate an active carbon/silica solid acid firmly loaded on the carrier.

4. CONCLUSION

In summary, a novel carbon/silica solid acid catalyst HS/C-SO₃H was prepared by a chemical activation method. Interestingly, the obtained solid acid catalyst exhibits more highly catalytic activity in the esterification of oleic acid with methanol compared to SBA-15/C-SO₃H and MCM-41/C-SO₃H. Compared to the long, two-dimensional mass-transport limiting channels of SBA-15/C-SO₃H and MCM-41/C-SO₃H, the unique structure of HS/C-SO₃H, i.e., the thin mesoporous shell with connected interior and exterior surfaces, acts as the highway for the enhanced mass-transport process. This strategy can produce a solid acid catalyst with favorable acid properties and good active site accessibility, which has a good application future in the field of green chemistry.

■ ASSOCIATED CONTENT

Supporting Information

The Supporting Information is available free of charge on the ACS Publications website at DOI: 10.1021/acsami.5b08797.

Additional experimental data including the TEM images, small-angle X-ray diffraction (SAXRD) patterns, TGA,

XRD patterns, NH₃-TPD profiles, element content measured by CHNS analysis, and S content and relative percentage of S-containing function groups obtained by fitting S 2p XPS spectra of prepared materials (PDF).

■ AUTHOR INFORMATION

Corresponding Authors

*N. Tsubaki. E-mail: tsubaki@eng.u-toyama.ac.jp. Tel/Fax: (+81)-76-445-6846.

*M. Wu. E-mail: wumb@upc.edu.cn. Tel: (+86) 532-86983452. Fax: (+86) 532-86981787.

Author Contributions

The paper was written through contributions of all authors. All authors have given approval to the final version of the paper.

Notes

The authors declare no competing financial interest.

■ ACKNOWLEDGMENTS

This work is supported by the National Natural Science Foundation of China (Nos. 51172285, 51372277, 51402192); the Fundamental Research Funds for the Central Universities (No.15CX08005A); State Key Laboratory of Heavy Oil Processing (SKLHOP201503).

■ REFERENCES

- Lee, A. F.; Bennett, J. A.; Manayil, J. C.; Wilson, K. Heterogeneous Catalysis for Sustainable Biodiesel Production via Esterification and Transesterification. *Chem. Soc. Rev.* **2014**, *43*, 7887–7916.
- Su, F.; Guo, Y. Advancements in Solid Acid Catalysts for Biodiesel Production. *Green Chem.* **2014**, *16*, 2934–2957.
- Park, J. Y.; Kim, D. K.; Lee, J. S. Esterification of Free Fatty Acids Using Water-Tolerable Amberlyst as a Heterogeneous Catalyst. *Bioresour. Technol.* **2010**, *101*, 62–65.
- Yan, S.; Salley, S. O.; Simon Ng, K. Y. Simultaneous Transesterification and Esterification of Unrefined or Waste Oils over ZnO-La₂O₃ Catalysts. *Appl. Catal., A* **2009**, *353*, 203–212.
- Chen, G.; Fang, B. Preparation of Solid Acid Catalyst from Glucose-Starch Mixture for Biodiesel Production. *Bioresour. Technol.* **2011**, *102*, 2635–2640.
- Guo, F.; Fang, Z.; Tian, X. F.; Long, Y. D.; Jiang, L. Q. One-Step Production of Biodiesel from Jatropha Oil with High-Acid Value in Ionic Liquids. *Bioresour. Technol.* **2011**, *102*, 6469–6472.
- Arata, K. Organic Syntheses Catalyzed by Superacidic Metal Oxides: Sulfated Zirconia and Related Compounds. *Green Chem.* **2009**, *11*, 1719–1728.
- Reddy, B. M.; Patil, M. K. Organic Syntheses and Transformations Catalyzed by Sulfated Zirconia. *Chem. Rev.* **2009**, *109*, 2185–2208.
- Melero, J. A.; Iglesias, J.; Morales, G. Heterogeneous Acid Catalysts for Biodiesel Production: Current Status and Future Challenges. *Green Chem.* **2009**, *11*, 1285–1308.
- Zhang, X.; Zhao, Y.; Xu, S.; Yang, Y.; Liu, J.; Wei, Y.; Yang, Q. Polystyrene Sulphonic Acid Resins with Enhanced Acid Strength via Macromolecular Self-Assembly within Confined Nanospace. *Nat. Commun.* **2014**, *5*, 3170–3178.
- Andrijanto, E.; Dawson, E. A.; Brown, D. R. Hypercrosslinked Polystyrene Sulphonic Acid Catalysts for the Esterification of Free Fatty Acids in Biodiesel Synthesis. *Appl. Catal., B* **2012**, *115*, 261–268.
- Zuo, D.; Lane, J.; Culy, D.; Schultz, M.; Pullar, A.; Waxman, M. Sulfonic Acid Functionalized Mesoporous SBA-15 Catalysts for Biodiesel Production. *Appl. Catal., B* **2013**, *129*, 342–350.
- Pirez, C.; Caderon, J. M.; Dacquin, J. P.; Lee, A. F.; Wilson, K. Tunable KIT-6 Mesoporous Sulfonic Acid Catalysts for Fatty Acid Esterification. *ACS Catal.* **2012**, *2*, 1607–1614.

- (14) Hoffmann, F.; Cornelius, M.; Morell, J.; Froba, M. Silica-Based Mesoporous Organic-Inorganic Hybrid Materials. *Angew. Chem., Int. Ed.* **2006**, *45*, 3216–3251.
- (15) Kulkarni, M. G.; Gopinath, R.; Meher, L. C.; Dalai, A. K. Solid Acid Catalyzed Biodiesel Production by Simultaneous Esterification and Transesterification. *Green Chem.* **2006**, *8*, 1056–1062.
- (16) Srilatha, K.; Issariyakul, T.; Lingaiah, N.; Prasad, P. S. S.; Kozinski, J.; Dalai, A. K. Efficient Esterification and Transesterification of Used Cooking Oil Using 12-Tungstophosphoric Acid (TPA)/Nb₂O₅ Catalyze. *Energy Fuels* **2010**, *24*, 4748–4755.
- (17) Su, D. S.; Perathoner, S.; Centi, G. Nanocarbons for the Development of Advanced Catalysts. *Chem. Rev.* **2013**, *113*, 5782–5816.
- (18) Titirici, M. M.; White, R. J.; Brun, N.; Budarin, V. L.; Su, D. S.; del Monte, F.; Clark, J. H.; MacLachlan, M. J. Sustainable Carbon Materials. *Chem. Soc. Rev.* **2015**, *44*, 250–290.
- (19) Hara, M.; Yoshida, T.; Takagaki, A.; Takata, T.; Kondo, J. N.; Hayashi, S.; Domen, K. A Carbon Material as a Strong Protonic Acid. *Angew. Chem., Int. Ed.* **2004**, *43*, 2955–2958.
- (20) Toda, M.; Takagaki, A.; Okamura, M.; Kondo, J. N.; Hayashi, S.; Domen, K.; Hara, M. Green Chemistry: Biodiesel Made with Sugar Catalyst. *Nature* **2005**, *438*, 178–178.
- (21) Liu, R.; Wang, X.; Zhao, X.; Feng, P. Sulfonated Ordered Mesoporous Carbon for Catalytic Preparation of Biodiesel. *Carbon* **2008**, *46*, 1664–1669.
- (22) Zhang, M.; Sun, A.; Meng, Y.; Wang, L.; Jiang, H.; Li, G. High Activity Ordered Mesoporous Carbon-Based Solid Acid Catalyst for the Esterification of Free Fatty Acids. *Microporous Mesoporous Mater.* **2015**, *204*, 210–217.
- (23) Gao, Z.; Tang, S.; Cui, X.; Tian, S.; Zhang, M. Efficient Mesoporous Carbon-Based Solid Catalyst for the Esterification of Oleic Acid. *Fuel* **2015**, *140*, 669–676.
- (24) Nakajima, K.; Okamura, M.; Kondo, J. N.; Domen, K.; Tatsumi, T.; Hayashi, S.; Hara, M. Amorphous Carbon Bearing Sulfonic Acid Groups in Mesoporous Silica as a Selective Catalyst. *Chem. Mater.* **2009**, *21*, 186–193.
- (25) Liu, Y.; Chen, J.; Yao, J.; Lu, Y.; Zhang, L.; Liu, X. Preparation and Properties of Sulfonated Carbon-Silica Composites from Sucrose Dispersed on MCM-48. *Chem. Eng. J.* **2009**, *148*, 201–206.
- (26) Valle-Vigon, P.; Sevilla, M.; Fuertes, A. B. Sulfonated Mesoporous Silica-Carbon Composites and their Use as Solid Acid Catalysts. *Appl. Surf. Sci.* **2012**, *261*, 574–583.
- (27) Wang, J.; Xu, W.; Ren, J.; Liu, X.; Lu, G.; Wang, Y. Efficient Catalytic Conversion of Fructose into Hydroxymethylfurfural by a Novel Carbon-Based Solid Acid. *Green Chem.* **2011**, *13*, 2678–2681.
- (28) Russo, P. A.; Antunes, M. M.; Neves, P.; Wiper, P. V.; Fazio, E.; Neri, F.; Barreca, F.; Mafra, L.; Pillinger, M.; Pinna, N.; Valente, A. A. Solid Acids with SO₃H Groups and Tunable Surface Properties: Versatile Catalysts for Biomass Conversion. *J. Mater. Chem. A* **2014**, *2*, 11813–11824.
- (29) Russo, P. A.; Antunes, M. M.; Neves, P.; Wiper, P. V.; Fazio, E.; Neri, F.; Barreca, F.; Mafra, L.; Pillinger, M.; Pinna, N.; Valente, A. A. Mesoporous Carbon-Silica Solid Acid Catalysts for Producing Useful Bio-Products within the Sugar-Platform of Biorefineries. *Green Chem.* **2014**, *16*, 4292–4305.
- (30) Jia, R.; Ren, J.; Liu, X.; Lu, G.; Wang, Y. Design and Synthesis of Sulfonated Carbons with Amphiphilic Properties. *J. Mater. Chem. A* **2014**, *2*, 11195–11201.
- (31) Schaefer, Z. L.; Gross, M. L.; Hickner, M. A.; Schaak, R. E. Uniform Hollow Carbon Shells: Nanostructured Graphitic Supports for Improved Oxygen-Reduction Catalysis. *Angew. Chem., Int. Ed.* **2010**, *49*, 7045–7048.
- (32) Zeng, Y.; Wang, X.; Wang, H.; Dong, Y.; Ma, Y.; Yao, J. Multi-Shelled Titania Hollow Spheres Fabricated by a Hard Template Strategy: Enhanced Photocatalytic Activity. *Chem. Commun.* **2010**, *46*, 4312–4314.
- (33) Wang, G. H.; Sun, Q.; Zhang, R.; Li, W. C.; Zhang, X. Q.; Lu, A. H. Weak Acid-Base Interaction Induced Assembly for the Synthesis of Diverse Hollow Nanospheres. *Chem. Mater.* **2011**, *23*, 4537–4542.
- (34) Liu, D. H.; Guo, Y.; Zhang, L. H.; Li, W. C.; Sun, T.; Lu, A. H. Switchable Transport Strategy to Deposit Active Fe/Fe₃C Cores into Hollow Microporous Carbons for Efficient Chromium Removal. *Small* **2013**, *9*, 3852–3857.
- (35) Guo, L.; Zhang, L.; Zhang, J.; Zhou, J.; He, Q.; Zeng, S.; Cui, X.; Shi, J. Hollow Mesoporous Carbon Spheres—an Excellent Bilirubin Adsorbent. *Chem. Commun.* **2009**, *40*, 6071–6073.
- (36) Fang, X.; Zhao, X.; Fang, W.; Chen, C.; Zheng, N. Self-Templating Synthesis of Hollow Mesoporous Silica and Their Applications in Catalysis and Drug Delivery. *Nanoscale* **2013**, *5*, 2205–2218.
- (37) Lu, A. H.; Sun, T.; Li, W. C.; Sun, Q.; Han, F.; Liu, D. H.; Guo, Y. Synthesis of Discrete and Dispersible Hollow Carbon Nanospheres with High Uniformity by Using Confined Nanospace Pyrolysis. *Angew. Chem., Int. Ed.* **2011**, *50*, 11765–11768.
- (38) Li, Y.; Shi, J. Hollow-Structured Mesoporous Materials: Chemical Synthesis, Functionalization and Applications. *Adv. Mater.* **2014**, *26*, 3176–3205.
- (39) Ikeda, S.; Ishino, S.; Harada, T.; Okamoto, N.; Sakata, T.; Mori, H.; Kuwabata, S.; Torimoto, T.; Matsumura, M. Ligand-Free Platinum Nanoparticles Encapsulated in a Hollow Porous Carbon Shell as a Highly Active Heterogeneous Hydrogenation Catalyst. *Angew. Chem., Int. Ed.* **2006**, *45*, 7063–7066.
- (40) Fang, X.; Liu, Z.; Hsieh, M. F.; Chen, M.; Liu, P.; Chen, C.; Zheng, N. Hollow Mesoporous Aluminosilica Spheres with Perpendicular Pore Channels as Catalytic Nanoreactors. *ACS Nano* **2012**, *6*, 4434–4444.
- (41) Joo, S. H.; Park, J. Y.; Tsung, C.-K.; Yamada, Y.; Yang, P.; Somorjai, G. A. Thermally Stable Pt/Mesoporous Silica Core-Shell Nanocatalysts for High-Temperature Reactions. *Nat. Mater.* **2009**, *8*, 126–131.
- (42) Galeano, C.; Meier, J. C.; Peinecke, V.; Bongard, H.; Katsouraros, I.; Topalov, A. A.; Lu, A. H.; Mayrhofer, K. J. J.; Schuth, F. Toward Highly Stable Electrocatalysts via Nanoparticle Pore Confinement. *J. Am. Chem. Soc.* **2012**, *134*, 20457–20465.
- (43) Qi, G.; Wang, Y.; Estevez, L.; Switzer, A. K.; Duan, X.; Yang, X.; Giannelis, E. P. Facile and Scalable Synthesis of Monodispersed Spherical Capsules with a Mesoporous Shell. *Chem. Mater.* **2010**, *22*, 2693–2695.
- (44) Zhao, D.; Huo, Q.; Feng, J.; Chmelka, B. F.; Stucky, G. D. Nonionic Triblock and Star Diblock Copolymer and Oligomeric Surfactant Syntheses of Highly Ordered, Hydrothermally Stable, Mesoporous Silica Structures. *J. Am. Chem. Soc.* **1998**, *120*, 6024–6036.
- (45) Wang, Y. J.; Wang, X. H.; Li, J.; Mo, Z. S.; Zhao, X. J.; Jing, X. B.; Wang, F. S. Conductive Polyaniline/Silica Hybrids from Sol-Gel Process. *Adv. Mater.* **2001**, *13*, 1582–1585.
- (46) Liu, X. X.; Li, Y. B.; Bian, L. J.; Dou, Y. Q.; Huo, Y. Q. Electrodeposition of Hybrid Film of Polyaniline/Silica and its Pseudocapacitive Properties. *J. Solid State Electrochem.* **2008**, *12*, 909–912.
- (47) Lee, H. I.; Joo, S. H.; Kim, J. H.; You, D. J.; Kim, J. M.; Park, J. N.; Chang, H.; Pak, C. Ultrastable Pt Nanoparticles Supported on Sulfur-Containing Ordered Mesoporous Carbon via Strong Metal-Support Interaction. *J. Mater. Chem.* **2009**, *19*, 5934–5939.
- (48) Poonjarernsilp, C.; Sano, N.; Tamon, H. Simultaneous Esterification and Transesterification for Biodiesel Synthesis by a Catalyst Consisting of Sulfonated Single-Walled Carbon Nanohorn Dispersed with Fe/Fe₂O₃ Nanoparticles. *Appl. Catal., A* **2015**, *497*, 145–152.
- (49) Geng, L.; Yu, G.; Wang, Y.; Zhu, Y. Ph-SO₃H-Modified Mesoporous Carbon as an Efficient Catalyst for the Esterification of Oleic Acid. *Appl. Catal., A* **2012**, *427*, 137–144.
- (50) Lou, W. Y.; Guo, Q.; Chen, W. J.; Zong, M. H.; Wu, H.; Smith, T. J. A Highly Active Bagasse-Derived Solid Acid Catalyst with Properties Suitable for Production of Biodiesel. *ChemSusChem* **2012**, *5*, 1533–1541.
- (51) Chang, B.; Fu, J.; Tian, Y.; Dong, X. Multifunctionalized Ordered Mesoporous Carbon as an Efficient and Stable Solid Acid

Catalyst for Biodiesel Preparation. *J. Phys. Chem. C* **2013**, *117*, 6252–6258.